Supplementary Information for
"Macroscopic magnetic frustration"
by P. Mellado, A. Concha and L. Mahadevan

S1. Coulomb like interaction between two magnetic rods

In order to compute the magnetic charge parameter q used in our simulations, we measured the force-distance relation for several bar magnets using an Instron 5544 system to estimate the charge (pole strength) at the end of each bar in the dumbbell model. Two magnetic rods of equal dimensions were aligned with respect to each other at a distance z along the vertical axis and with opposite poles facing each other. Then, one of the rods was pulled apart and the interaction force measured, with a typical outcome shown in Figure S1, where the experimental data for two rods in the configuration shown in the inset of Figure S1 is shown in red. The continuous black line is the fit obtained from a dumbbell model, where interactions between magnetic poles follow a Coulomb law, and the only free parameter is the magnetic charge at the tips of the rod:

$$F(z) = \frac{\mu_0 q^2}{4\pi}\left(\frac{1}{z^2} - \frac{2}{(z+2a)^2} + \frac{1}{(z+4a)^2}\right) \tag{S1}$$

From the fit $F(z)$ we found $q = 2.03 \pm 0.08$ A m, in good agreement with previous estimates [1]. For a rod of radius $r = d/2$, $q = M_s \pi d^2/4$ [1], using this result we computed the saturation magnetization as $M_s = (1.21 \pm 0.03) \times 10^6$ A m^{-1} which is in agreement with the available data of the magnetization of Neodymium rods, validating the dumbbell approximation when the rods are separated by a distance $z > d$, as previously pointed out [2–4].

S2. Moment of Inertia, Static friction and Damping coefficient.

The moment of inertia of magnetic rods around their local rotation axis is $I = ML^2/12$, where M is the rod mass (assuming uniform density) and L its length. The extra moment of inertia given by the plastic holder of mass m, is negligible as it is short and light $m \sim 0.05 \times 10^{-3}$ Kg. The mass of the magnetic rods used was measured individually for 50 random rods which yielded: $M = (0.278 \pm 0.003) \times 10^{-3}$ Kg. From this data we computed $I_0 = 8.41 \times 10^{-9}$ Kg m^2. This value is used as input in the numerical simulations.

We quantified the static friction on each rotor, by placing a single rod at the center of a Helmholtz coil, as illustrated in Figure S2 and measured the critical field at which the rod deviates from its initial position to find $B_c = (2.4 \pm 0.1) \times 10^{-4}$ T. Using B_c we obtained the critical torque for which the rod starts to move and found that $T_c = 2aqB_c \sim 0.93 \times 10^{-5}$ N

m. The earth magnetic field plays not significant role being one order of magnitude smaller than B_c.

To compute the damping coefficient η, we isolated a single rotor and impulsively applied a torque to it, and then recorded its relaxation dynamics using a Phantom V7.3 high speed camera with frame rates between 1000 fps (frames per second) up to 4000 fps. Using standard imaging techniques we extracted the evolution of $\alpha(t)$, which corresponds to a damped dynamics in absence of external forcing. The damping is computed directly by fitting it to the solution $\alpha \sim \exp(-t/\tau_D)$, (Fig. S3) and thus we estimated the damping time of a single rod to be $\tau_D = 0.83 \pm 0.18$ s.

S3. Single rod Dynamics and Triad

A magnetic bar of length $L = 2a$ and diameter $d \ll 2a$, behaves like two magnetic monopoles of equal strength but opposite sign located at each end of the bar [2, 3]. The magnetic moment of each magnet is then given by $|\mathbf{m}| = 2aq$, where $2a\hat{\mathbf{r}}$ is the vector separating the two poles and $\mathbf{m}$ points from S to N, so that poles of two distinct rods interact through Coulomb's law[2, 3]. The dynamics of a single rotor can be understood by examining its response to a uniform magnetic field along the $\hat{z}$ direction, with an equation of motion given by:

$$I\frac{d^2\alpha}{dt^2} = T_e - \eta\frac{d\alpha}{dt} \tag{S2}$$

where I is the rotational moment of inertia of the rod (Supplementary S2), η is the damping coefficient of the hinge, and $T_e = 2aqB_0 \sin(\alpha)$ is the torque due to the action of an external magnetic field on the localized charges at the end of the rod. This simplified system has two natural time-scales: an inertial time $\tau_B = 2\pi(I/2a|qB_0|)^{1/2} \sim 0.003/|B_0|^{1/2}$ and a frictional time $\tau_D = I/\eta \sim 1s$. Since $\tau_B = \tau_D$ for a critical field $B_0^* \sim 10^{-6}$ T, the dynamics of a single rod is underdamped in all our experiments.

The minimal model where Coulomb interactions produces frustration in our system arises in the unit cell of three magnetic rods of length L at 120°, that is frustrated in the plane. When $\Delta/L < 0.2$ the rods lie in the $x - y$ plane in a spin ice configuration as shown in Figure S4; as Δ/L is increased, the out of plane magnetization of the triad M_z increases (Fig. S4), while when we reverse this operation, hysteresis is observed, a consequence of

static friction in the system (see Fig. S11a for M_z versus Δ/L in the lattice). We have used a single triad to examine the role of geometrical disorder by measuring M_z when one of the hinges was rotated in the plane by $\delta\theta$ (Figure S4 inset). We observe that the system remains in the $x-y$ plane for small $\delta\theta$; however, when $\delta\theta \sim 35^\circ$ M_z starts to increase rapidly until $\delta\theta \sim 50^\circ$ when one magnet becomes almost perpendicular to the plane.

The relaxation dynamics of the lattice made of unit cells is strongly dependent on the strength of the interactions and thus on the lattice parameters. For example, the damping time $\tau_D^{\rm triad}$ of one of the rotors belonging to a triad grows with Δ (Fig. S5). When the $\Delta/2a$ approaches the lattice parameters, the dynamics of one rod in the triad approaches that of a rod in the lattice. Indeed when $\Delta/2a < 0.2$, we found $\tau_D^{\rm triad} \sim 0.04$ s, close to the relaxation time of a single rotor in the lattice, $t_{\rm rel} \sim 0.034$ s, which was found by computing the experimental single-particle autocorrelation function $C(t) = (\langle m_i(t)m_i(0)\rangle - \langle m_i\rangle^2)/(\langle m_i^2\rangle - \langle m_i\rangle^2)$ averaged over all rotors, and fitting its first 0.08 seconds of evolution to an exponential decay as shown in Figure S6.

S4. Experimental Lattice

All 352 rods were made out of Neodymium (NdFeB plated with three layers: Ni-Cu-Ni), with saturation magnetization $M_s = 1.2 \times 10^6$ A m^{-1}, length $L = 2a = 1.9 \times 10^{-2}$ m, diameter $d = 1.5 \times 10^{-3}$ m and mass $M = 0.28 \times 10^{-3}$ Kg. They were hinged at the plane that is equidistant from their N and S magnetic poles, such that their axis of rotation crosses their center of mass. The hinges were made out of Acrylic-based photopolymer FullCure720 (Transparent) using a 3D printer Connex500 from ObJet Geometries. The hinges supporting the rods were introduced at the holes of an acrylic plate of size 0.61×0.61 m, defining the sites of a kagome lattice with lattice constant $l = \sqrt{3}(a + \Delta)$ where $\Delta = 4.675 \times 10^{-3}$ m. There was a small amount of geometrical disorder in the azimuthal orientation of the rotors, θ, due to lattice imperfections $\delta\theta_{\rm max} \sim 2^o$. We measured the azimuthal deviations of the rotors in the lattice when they were in the planar $(x-y)$ configuration from lattice pictures (see below) to find that they follow a Gaussian distribution with mean $\bar{\delta\theta} = 1.2^\circ$

The number of rods, and their positions in the lattice were unchanged between experiments otherwise mentioned. To examine the configurations of the system, we took high-resolution pictures out of ten different experimental realizations, and used standard imaging

techniques to obtain $2D$ maps with the positions of each magnetic pole (South poles colored black). Each realization was accomplished after perturbing the lattice with an external dipole in order to produce a different initial and final magnetic state. In every occasion all vertices satisfied the ice rule. Away from the edges of the system, the spin ice rule was very robust, though small out of plane deviations larger than $\delta\alpha$, were sometimes observed at the edges of the lattice, a feature that becomes increasingly irrelevant for large systems. The averaged value of the total normalized magnetization of the sample, along x and y directions typically achieved $\langle m_x \rangle \sim 0.12$ and $\langle m_y \rangle \sim -0.182$ respectively.

Correlations

In order to obtain the evolution of the nearest neighbor magnetic correlations in time, rotors were polarized using a Solenoid of 850 Turns with length 0.1 m and radius $r = 0.4$ m made out of copper wire of diameter $d = 0.51$ mm. The lattice was located inside the solenoid at its medial plane so that the radial component of the field was zero. The coil was connected in series with an ammeter and a regulated dc power supply serving as a current source. We used currents up to $i = 3.5$ A to create a magnetic field strong enough to polarize our sample. At $i = 1.5$ A, ($B_z \sim 3.2 \times 10^{-3}$ T), all the N poles of the rods were pointing along the $\hat{z}$ direction. Next we turned the field off and waited until the rotors relaxed, simultaneously recording the evolution of the rods with a high speed Phantom V9.0 camera. We then analyzed these data using standard imaging techniques and extracted the full time trajectory, $\alpha_i(t)$, of each rod i from movies like the one shown in Supplementary SM1.

The three dimensional evolution of the rods is characterized by the vector

$$\vec{m}_i(t) = (\cos\theta_i \sin\alpha_i(t), \sin\theta_i \sin\alpha_i(t), \cos\alpha_i(t)) \,.$$

thus the evolution of nearest neighbor rods correlations reads $S_{\alpha\beta}(t)\langle \vec{m}_i \cdot \vec{m}_{i+1} \rangle(t) = (1/n) \sum_i \vec{m}_i(t) \cdot \vec{m}_{i+1}(t) / |\vec{m}_i(t) \cdot \vec{m}_{i+1}(t)|$. A coarse grained charge at vertex k, at any time t, can be defined by $Q_k(t) = \sum_{i=1}^{3} q_i \cos\alpha_i(t)$. First, second and third nearest neighbors magnetic correlation as well as nearest neighbor charge correlations after relaxation are summarized in Figure S8.

Lattice dynamics

The fastest time scale of lattice relaxation is dominated by Coulomb interactions at the very onset of motion where all rods are in a configuration with their **S** poles pointing along the $\hat{z}$ direction. During the first 0.07 seconds, two sublattices reach the plane before the remaining sublattice and organize in head to tail chains showing trend to ferromagnetic order. The experimental nearest-neighbor correlation decays exponentially, with a characteristic Coulomb time scale $t_c = 0.02$ seconds. To understand this, we compute $\alpha(t)$ for a single rod using equation S2, where torques are due to Coulomb interactions with neighbors oriented at 120° relative to each other in the chains along the $\hat{y}$ direction. The numerical solution of this minimal model allows us to find that $\cos(\alpha(t))$ decays exponentially with characteristic time equal to t_c. At leading order in α, it also gave us a good estimate for $t_c = \frac{2^{3/4}}{q}\sqrt{4\pi I a/\mu_0} =$ 0.02 s.

Once all the rods reach the $x-y$ plane, the next relaxation stage involves the rotation of the rods around their center of mass. The amount of time rotations last in the system can be found by numerically solving the nonlinear differential equation of a damped rotor which rotate due to the torque generated by Coulomb interactions with its four nearest neighbors located at 120° of each other in a mean field approximation:

$$\alpha''(t) = \Omega_b^2 \sin(\alpha(t)) - \Omega_\eta \alpha'(t) \tag{S3}$$

, with initial conditions $\alpha(0) = 0$, $\alpha'(0) = V$, where V is obtained from energy conservation at the onset of the rotor dynamics, $\Omega_b = \sqrt{2qa\langle B\rangle_{rms}}$, $\Omega_\eta = \eta/I \sim 1$ seconds and $\langle B\rangle_{rms}$ is the internal magnetic field due to the Coulomb interaction with its neighbors averaged over a cycle. For our experimental parameters, the phase space trajectory changes from open orbits into a dissipative attractor after 0.45 seconds: during this time the rotors average about 4 full rotations before they begin to oscillate as shown in Figure S7. As expected, this simplified model does not reproduce all details of the collective dynamics. However, it captures well the typical time scales for full librations and oscillatory behavior expected before the collective ground state is reached. To resolve the effect of collective dynamics we solved the equations of damped motion for each rotor Coulomb interacting with all the other rotors in the system using molecular dynamics simulations as described in section S5.

Phase diagram

To characterize the response of the system to external perturbations, we built a cart that can carry dipoles of length $L^e = 0.135$ m, cross section radius $r^e = 6.35 \cdot 10^{-3}, 3.18 \cdot 10^{-3}, 1.59 \cdot 10^{-3}$ m and charges $Q^e = 64q, 16q$ and $8q$ respectively. This cart moves underneath the lattice with speed v between $1 - 7$ m/s, set by the initial impulse provided to the device (inset Fig. S9a). The second experimental variable was the distance between the closest point of the dipole to the lattice, h, which varied between 0.42 to 0.05 m. In each realization we start with a different magnetic configuration where rotors lie at the $x - y$ plane at not apparent magnetic order. The magnetic configuration is a result of agitating the relaxed lattice moving an external dipole randomly underneath the lattice. Then from the middle of the left boundary of the sample, a dipole with magnetic charge Q^e and length L^e and of strength $B_{ext} \sim Q^e/h^2$, crossed the sample at a speed v from one lattice edge to the other. In order to distinguish between inertial and interaction regime, we quantified the response of the system computing the root mean square fluctuation (RMSF) in α, about the rod's $x - y$ equilibrium position. This Lindemann like index $\delta_{Li} = \sum_{i,j} \frac{\sqrt{|\langle \mathbf{m_i m_j} \rangle_t^2 - \langle (\mathbf{m_i m_j})^2 \rangle_t|}}{|\langle \mathbf{m_i m_j} \rangle_t|}$, quantifies the angular fluctuations in the context of the parameters of the system, where $\langle \rangle_t$ means the temporal average. The threshold value of the Lindermann parameters $\delta_{Li}^{th} = 0.5$. When $\delta_{Li} < \delta_{Li}^{th}$, the system is in an inertial regime. The boundary between interaction and inertial regimes can be obtained using a single particle approximation by equating the impulse a rotor feels when the external dipole is moving at speed v, at a distance $d(t) = \sqrt{h^2 + (vt)^2}$, from it, to the change in the angular momentum of the rotor: $\delta L = \int (F(t) \times a) dt$, where $F = \mu_0 q Q^e/(h^2 + (vt)^2)$. Integrating over time in the right side between $-\beta/v$ and β/v, where $\beta = \sqrt{(h^{*2}h)^{2/3} - h^2}$, yields the change in the angular momentum of the rod due to its interaction with the upper charge of the dipole: $\delta L \sim \mu_0 q Q^e a/(2\pi h I v)$ (h^* is the threshold height for which the Coulomb interaction between a rod and the external dipole overcomes the static friction, as explained in the paper). For an arbitrary size of oscillations, δ_{Li}^{th}, we can get an estimation of how h change with v by integrating over time at the left side of the previous equation to get : $h \sim h^* (\mu_0 Q^e q a/I)^{3/2}/v^3$, which gives good account of experimental results. The interplay between the ratio of internal to external magnetic forces and the speed of the dipole, determines in average the oscillations amplitude in a belt of the sample whose width D can be computed in the quasi-static

approximation (Fig. S9), in terms of local interactions, static friction, and interactions with the top charge of the external dipole yielding $D/h^* \sim \sqrt{(h/h^*)^{2/3} - (h/h^*)^2}$, when $h < h^*$.

S5. Molecular Dynamics simulation

Numerical results were obtained by direct numerical integration of the equations of motion for each rod interacting with all the others 351 rotors via Coulomb interactions in the dumbbell picture using a Verlet method with an integration time step $\Delta t = 10^{-4}$ at zero temperature. In all simulations experimentally measured parameters for lattice constant, damping, inertia and charge of the rotors were used. Equilibration was accomplished after 2 seconds of real time lattice evolution (2×10^4 time steps). To check the system size dependence on the calculated quantities, we compared our results with those for a system with $n = 900$ rods. As there was no significant difference in the results between the $n = 900$ and $n = 352$ systems, we used the later number for all our simulations.

$$I\frac{d^2\alpha^{(i)}}{dt^2} = T_e^{(i)} - \eta\frac{d\alpha^{(i)}}{dt} \quad \text{,where:} \tag{S4}$$
$$T_e^{(i)} = \left(\frac{a\mu_0}{4\pi}\right)\sum_{j\neq i} q_i q_j \hat{r}_i^{cm} \times \frac{\vec{r}_{ij}}{|\vec{r}_{ij}|^3}$$

$\vec{r}_{ij}$ is the vector joining charges q_i and q_j, and $\hat{r}_i^{cm}$ is the unit vector pointing from the center of mass (cm) of the rod where charge q_i belongs. We find that the numerical lattice always fulfills the spin ice rules as shown in Figure S10. Correlations after equilibration compared with the experimental values (Table of Fig. S8), show that nearest and second neighbor correlations compare well while third neighbors and charge correlations are smaller than in the experimental counterpart. We attribute this to the absence of static friction in the numerical model. To complement the experimental phase diagram we performed simulations using a point-like magnetic charge $Q^e = 64q$, moving in a slightly larger parameter space (Σ) that the one experimentally explored , $\Sigma = (0.005, 10) \times (0.05, 0.5)$. Our numerical constructed findings in the inertial and interaction regimes fall inside the experimental one, showing that the basics physics is captured well by the numerical model.

Molecular dynamics simulations also permitted the examination of the out of plane lattice fluctuations versus variations in Δ/L. Figure S11a shows the lattice RMS deviations out of the $x - y$ plane averaged for all the n rods of the lattice $M_z\text{rms} = \sqrt{\sum_\text{i}(\cos\alpha_\text{i}{}^2)}/\text{n}$

growing linearly for $\Delta < 0.3L$. They show a behavior qualitatively similar to the total M_z of three dumbbells interacting via Coulomb, in a star configuration, obtained from energy minimization, Figure S11b for $\Delta < 0.4L$. An extended numerical study will be published elsewhere.

S6. Theory: Dipoles v/s Dumbbells

Once all rotors were placed in the kagome lattice, we found that the honeycomb spin ice phase is very robust: any time a rotor located at the bulk was displaced with our finger tips, it came back to the $x-y$ plane after a few oscillations. When we displaced it strongly so that a rotor flipped, locally new configurations in the spin ice manifold formed from sequential first-nearest-neighbor flips alone. Sequentially flipped second-nearest neighbor pairs were never observed, unless linked by a shared first nearest neighbor. Rotors being part of a closed magnetic loop were particularly stiff to external perturbations thus; single-particle spin-flipping suggests that flipping dynamics depends on local magnetic configurations.

We examined two limit cases in order to understand these findings. In the first one, we let the magnets lie far apart ($\Delta/a > 0.4$) so that a Hamiltonian with nearest neighbors dipolar interactions is a good approximation [2–4]. We found that the dipoles having a continuous U(1) symmetry, along their local axis prefer configurations in the $x-y$ plane in the honeycomb spin ice manifold. The ground state energy is degenerate, $E = -\frac{7D}{8}N_t$, where N_t is the total number of triangles of the kagome lattice and $D \sim O(a/\Delta) \sim 10^{-5}$ J, sets the energy scale for interactions. The cost of raising a rod is $\delta E = \frac{7D}{2}$, decreasing as Δ increases. This model also provides an easy estimation of the local energy configurations for a triad of rotors shown in Figure S1 where the ones satisfying the spin ice rule are energetically favorable since head to tail magnetic configurations are energetically favorable ($-1.75D$ instead of $1.75D$ of tail to tail or head to head configurations) which explains also why magnets taking part of closed loops are particularly stable to perturbations.

In the opposite limit, relevant for our experiments, rotors are brought close to each other such that $\Delta/a < 0.4$, and thus a dumbbell model is a reasonable description [3]. The ground state of our system can be understood in terms of magnetic dumbbells with magnetic charges at the ends of each rod. For a single triad of dumbbell dipoles, each having a length $2a$ and a charge of magnitude $\pm q$ on each dipole head and tail respectively, the full Coulomb

interaction between magnetic charges contains 12 terms and an arbitrary constant that represents the self energy of this system. The minimal distance between the origin and the closest charge is Δ, therefore in the limit $\Delta \to 0$ the energy will be given only by the three divergent Coulomb terms due to the interactions between the three charges $1, 2, 3$, that are closest to the origin. Thus, at leading order, the interaction energy is given by $U_\Delta \sim U_{12} + U_{23} + U_{31}$, where U_Δ is clearly divergent. In the same spirit as in QED and QCD [5], we describe the basic physics by paying attention only to the most divergent quantities and can understand the optimal charge configuration using the fact that $U_\Delta \sim g/\Delta$. Thus minimizing the Coulomb energy is equivalent to minimizing g. In the limit when $\Delta \to 0$, a is the only length scale. Then the leading order term in g will only depend on the geometry, and any needed change in the sign of the charge product will appear as a π change in the polar rotation angle. Therefore in considering the lowest energy configuration of three interacting dumbbells that are at a distance Δ from each other, we find that:

$$
\begin{aligned}
&g(\alpha_1, \alpha_2, \alpha_3) = \\
&(5 + \cos\alpha_1 \cos\alpha_2 - \sin\alpha_1 \,(-3 + \sin\alpha_2) - 3\sin\alpha_2)^{-1/2} + \\
&(5 + \cos\alpha_1 \cos\alpha_3 + \sin\alpha_1 \,(3 + \sin\alpha_3) + 3\sin\alpha_3)^{-1/2} + \\
&(5 - \cos\alpha_2 \cos\alpha_3 - \sin\alpha_2 \,(3 + \sin\alpha_3) + 3\sin\alpha_3)^{-1/2}
\end{aligned}
$$

where α_i are the rotation angles measured relative to the vertical axis (polar angle). The global minimum for $g(\alpha_1, \alpha_2, \alpha_3)$ occurs for planar configurations corresponding to the spin ice case, i.e. $(\alpha_1, \alpha_2, \alpha_3) = \pm(\pi/2, \pi/2, -\pi/2)$ or permutations. Thus, the basic building blocks of our experiment follow spin ice rules as the shortest distance between magnetic poles goes to zero asymptotically: the initial $U(1)$ symmetry for each rotor is reduced into a Z_2 Ising like symmetry.

Movies

Caption Movie SM1

Experimental lattice dynamics. In the initial state all the S poles of the lattice n rotors are pointing along $\hat{z}$. At $t = 0$, the magnetic field is switched off and the lattice relaxes over a period of 2 seconds. This dynamical process is shown here along with the

evolution of the nearest neighbor magnetic correlations. In the final state all the magnets lie in the $x - y$ plane in a honeycomb spin ice magnetic order.

Caption Movie SM2

Computational lattice dynamics. In the initial state all the S poles of the lattice n rotors are pointing along $\hat{z}$. At $t = 0$, the magnetic field is switched off and the lattice relaxes over a period of 2 seconds. This dynamical process is shown here along with the evolution of the nearest neighbor magnetic correlations. In the final state all the magnets lie in the $x - y$ plane in a honeycomb spin ice magnetic order.

[1] O. Tchernyshyov, Nature Physics **6**, 323 (2010).

[2] D. Vokoun, G. Tomassetti, M. Beleggia, and I. Stachiv, Journal of Magnetism and Magnetic Materials **323**, 55 (2011).

[3] D. Vokoun, M. Beleggia, L. Heller, and P. . ittner, Journal of Magnetism and Magnetic Materials **321**, 3758 (2009).

[4] T. H. Boyer, Am. J. Phys. **56**, 688 (1988).

[5] M. Franz, T. Pereg-Barnea, D. E. Sheehy, and Z. Tešanović, Phys. Rev. B **68**, 024508 (2003).

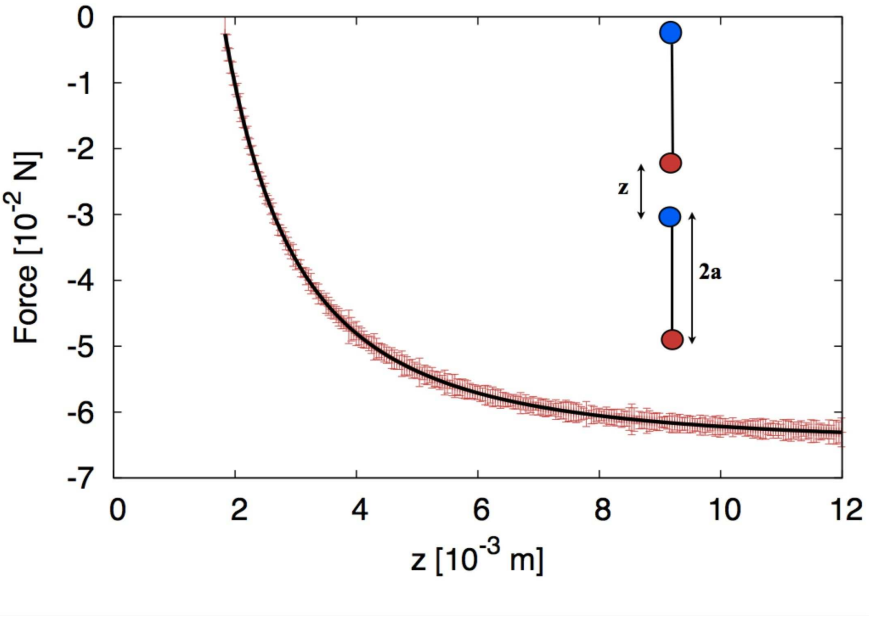

FIG. S1: Force vs. distance between two Neodymium rods. In red are shown the experimental data with error bars of the attractive force between two magnetic rods, as a function of the distance between the two closest faces of the rods. Black line represents the best fit obtained by using the Coulomb law (Eq.(S1)), from where we obtained the magnitude of the magnetic charges $q = 2.03 \pm 0.08$ A m. The inset illustrates a typical tensile experiment.

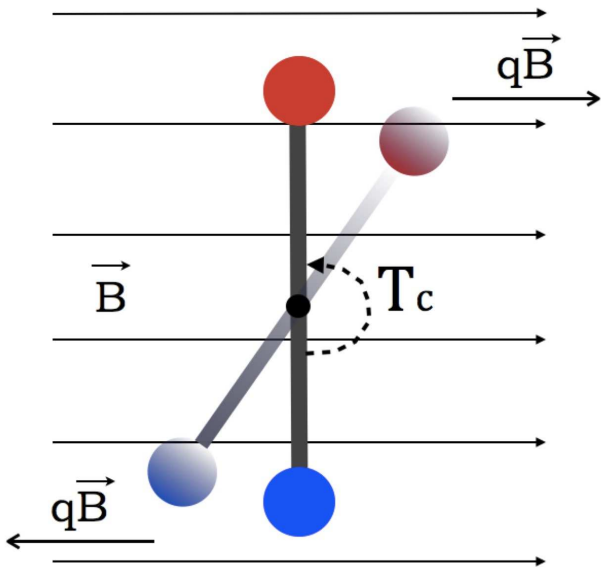

FIG. S2: Schematic of the setup used to measure static friction. A uniform magnetic field is applied to a single rod producing a torque in each of its poles. Once the rod depart from its equilibrium position we recorded the value of the magnetic field and computed T_c.

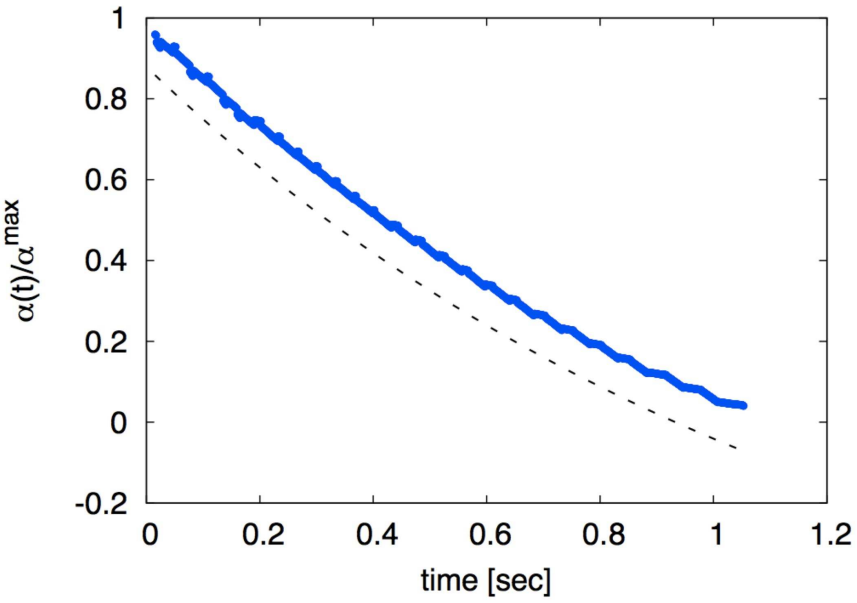

FIG. S3: Single rod dynamics. In blue are the experimental data taken from standard imaging techniques and the dashed black is the best fit obtained using an exponential damping model, offset by 0.1 for clarity purposes.

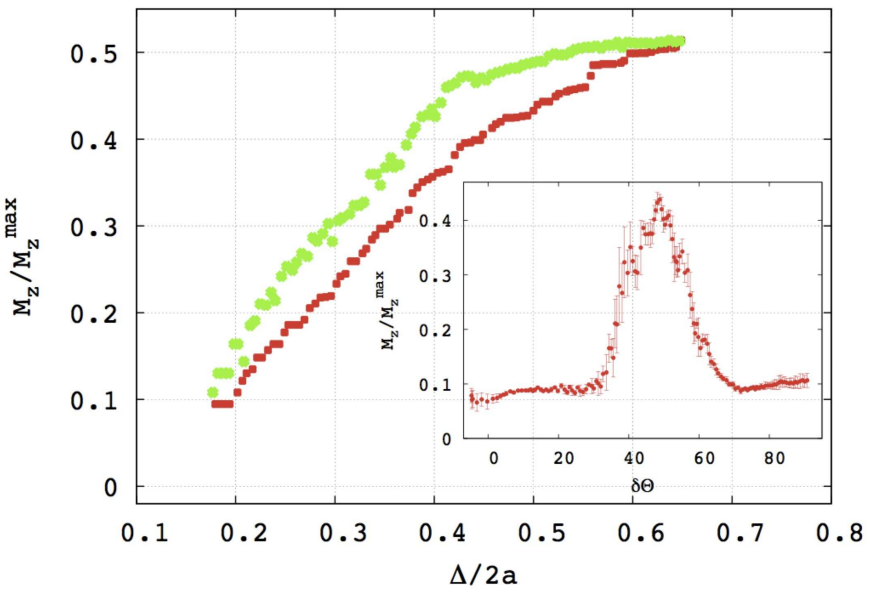

FIG. S4: Δ and θ dependence of the normalized magnetization for three rods in a 120° star configuration. M_z grows with $\Delta/2a$ and when the operation is reversed, the system shows hysteresis. The inset shows M_z growing when one of the rotors change its azhimutal orientation respect to the others by $\delta\theta$

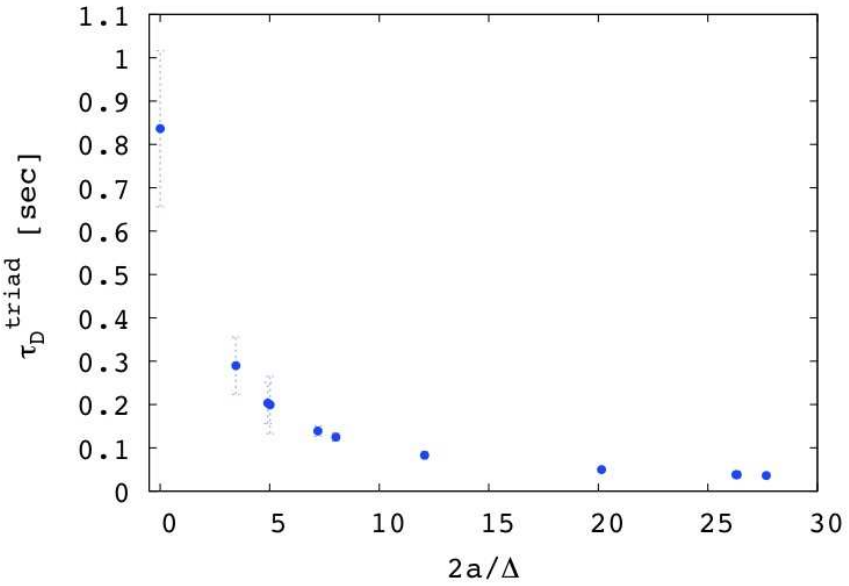

FIG. S5: τ_D^{triad} versus 2a/Δ. The relaxation time of a single rotor in a triad configuration with two nearest neighbors. $\tau_D^{triad} \sim t_{rel}$, when $2a/\Delta < 0.2$. The data $2a/\Delta = 0$ is the damping time of a free rod, τ_D.

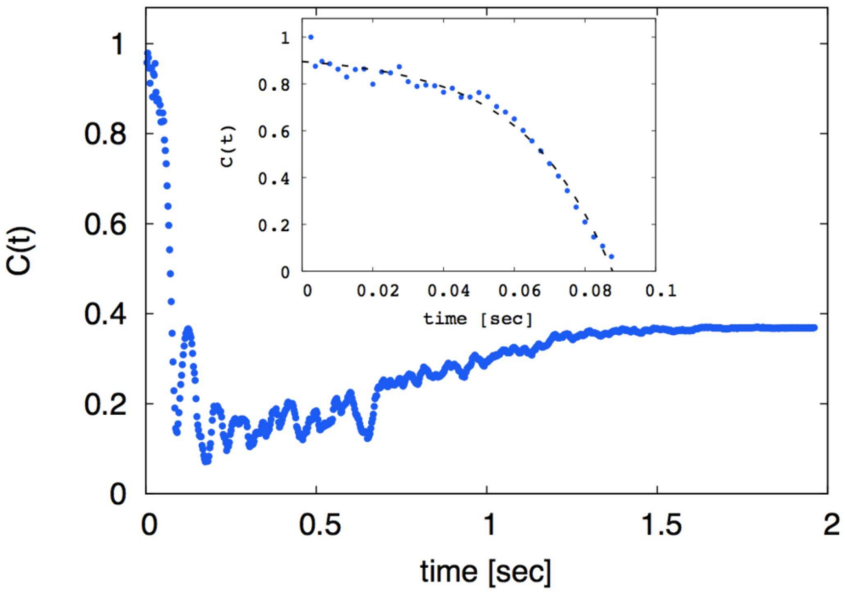

FIG. S6: Single particle autocorrelation, C(t). The (blue) points were obtained by computing the experimental single-particle autocorrelation function $C(t) = (\langle m_i(t)m_i(0)\rangle - \langle m_i\rangle^2)/(\langle m_i^2\rangle - \langle m_i\rangle^2)$ averaged over all rotors. Inset: $C(t)$ for the first 0.08 seconds of lattice relaxation (blue) compared with the function $\cos(\exp(-t/t_{rel}))$ which is the the best fit for C(t) (dashed black curve). From the fit we obtained the relaxation time of a single rotor in the lattice $t_{rel} = 0.034$ sec.

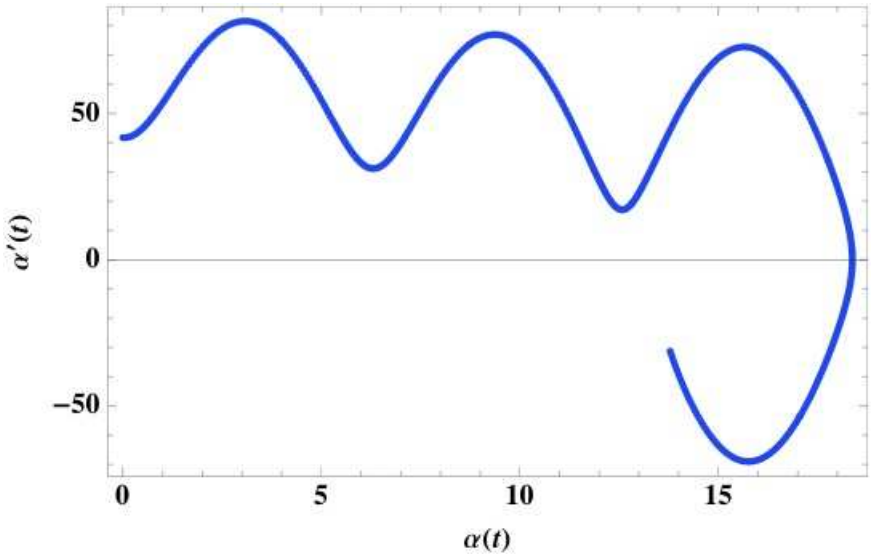

FIG. S7: Lattice dynamic at stage II. The phase space trajectory corresponding to the solution of equation S3 for a single rotor interacting with its four neighbors, after 0.45 seconds have elapsed.

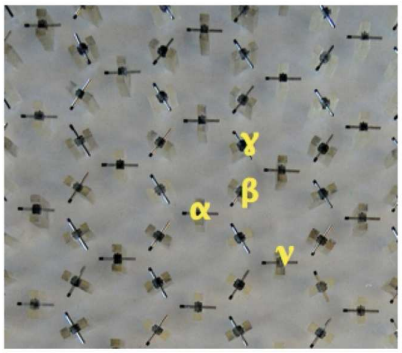

Correlation	Experiments	Simulations
$S\alpha\beta$	0.326 +/- 0.002	0.322 +/- 0.002
$S\alpha\gamma$	0.09 +/- 0.06	-0.18 +/- 0.05
$S\alpha\nu$	0.45 +/- 0.09	0.20 +/- 0.05
$C\alpha\beta$	-0.223 +/-0.001	-0.14 +/- 0.02

FIG. S8: Correlations after relaxation. Top: The honeycomb structure formed by connecting the spins of the kagome lattice. Each bar element represents a rod oriented along the axis. The Greek symbols label spins for correlation calculations. **Bottom:** First, second and third nearest neighbors magnetic correlation and nearest neighbors charge correlations for the experimental and numerical lattices.

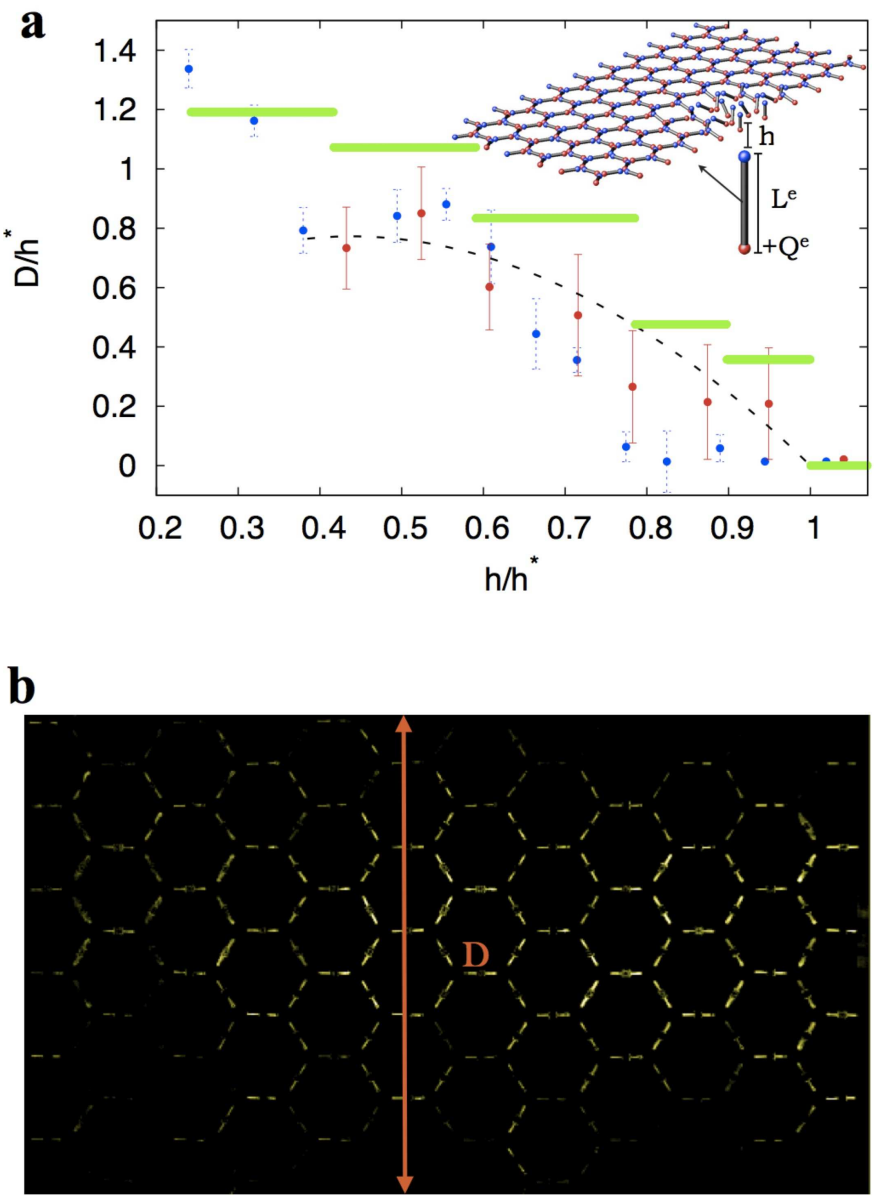

FIG. S9: D/h^* **v/s** h/h^***. a,** Experimental data showing the width D of the stripe of the sample which is excited due to two dipoles of charges $Q^e = 16q$ (blue) and $64q$ (red), in good agreement with the theoretical scaling (black dots) and the results from simulations (green) for $Q^e = 64q$. The inset illustrates the experiment, where a dipole of length L^e and charge Q^e located at distance h from the lattice is exciting a stripe of magnetic rods. **b,** Superimposed images obtained by computing the intensity difference between frames when the lattice is excited by an external dipole and a typical image from where we obtained experimental data for D.

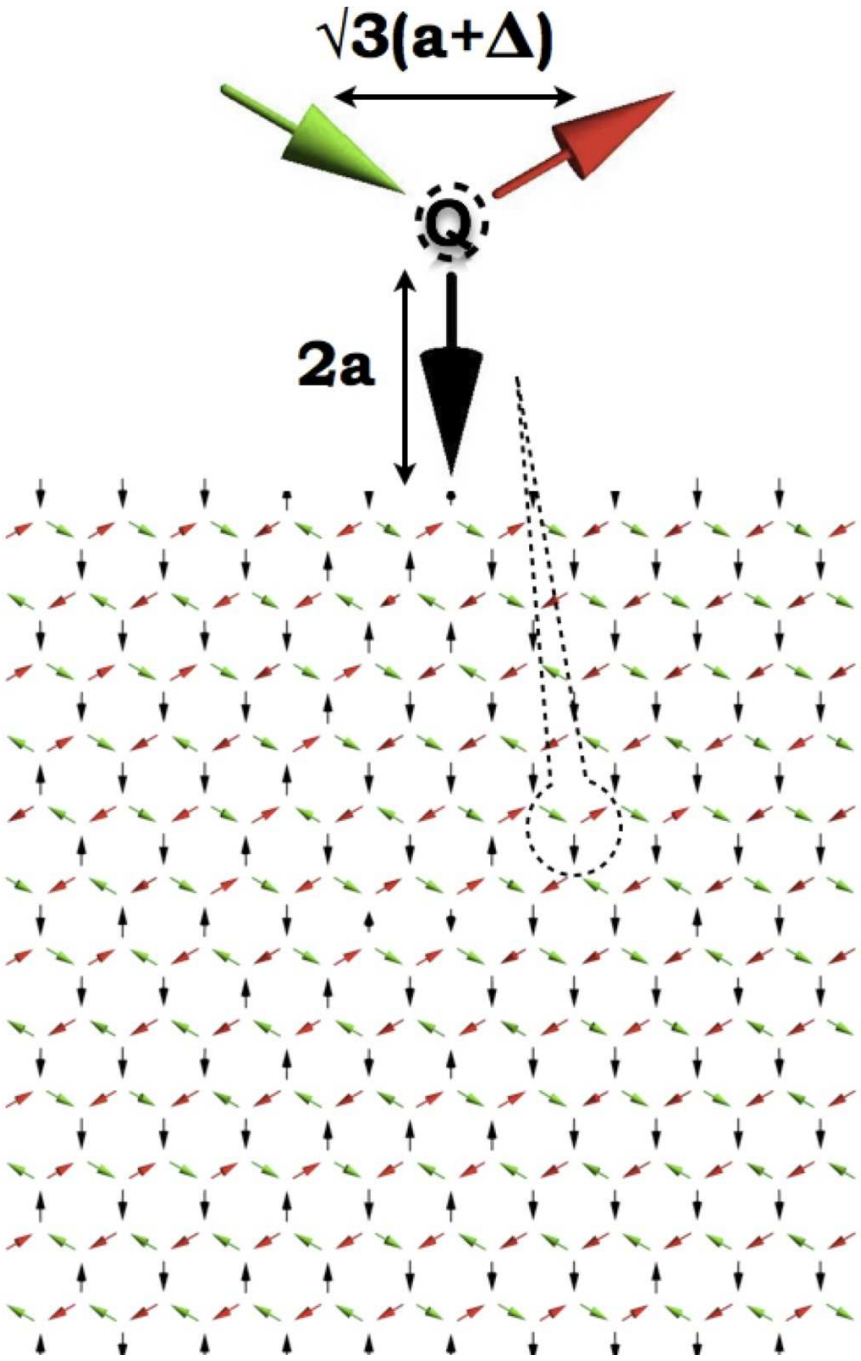

FIG. S10: Numerical lattice: Rods in a typical configuration fulfilling spin-ice rules after the numerical lattice has reached relaxation.

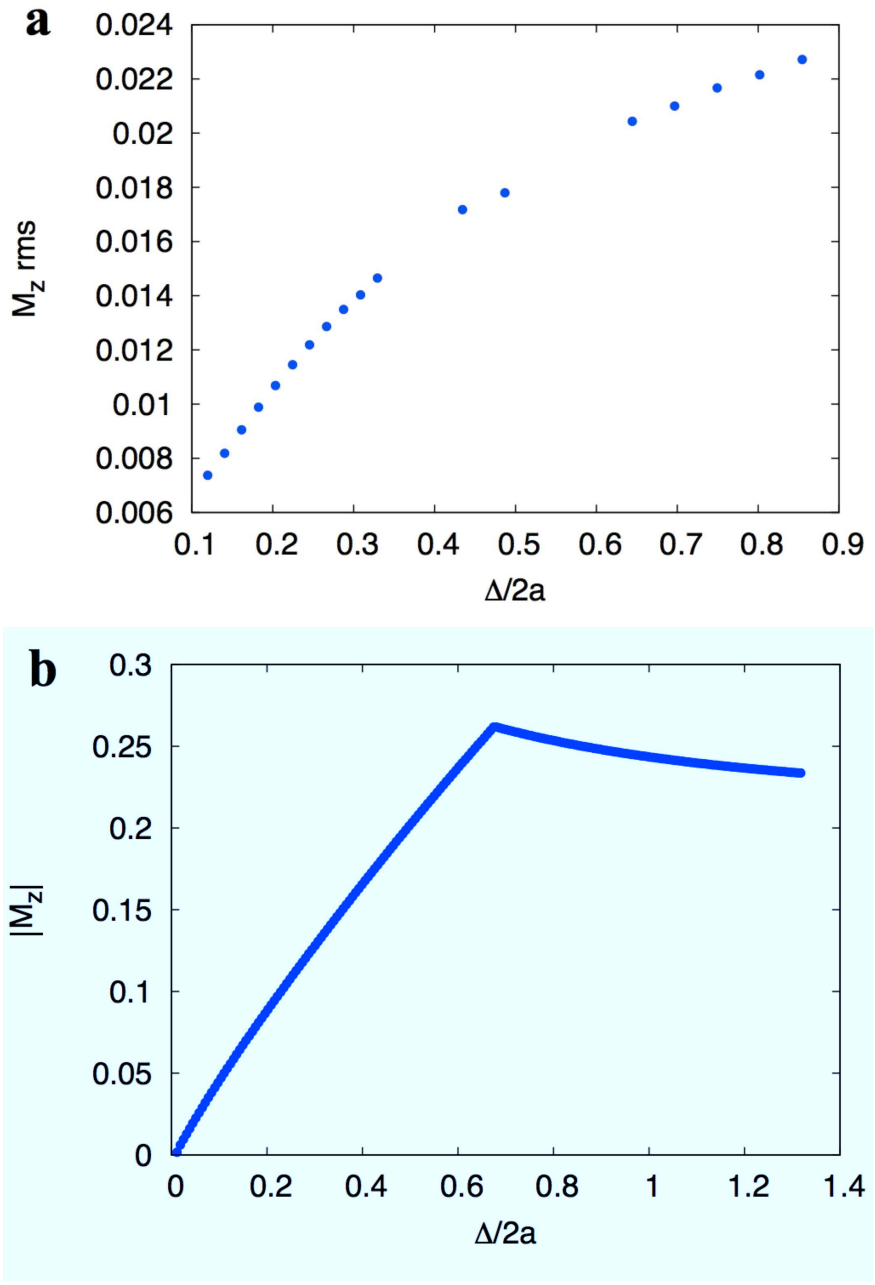

FIG. S11: Numerical M_z v/s Δ.a, RMS deviations out of the $x-y$ plane averaged for all the n rods of the lattice $M_z rms$ v/s $\Delta/2a$ after 4 seconds of simulation have elapsed. As the distance between nearest poles increases, rotors are more prone to choose positions which depart from the $x-y$ plane at equilibrium. **b,** Average magnetization along the z direction of a triad of rotors v/s $\Delta/2a$. M_z was obtained computing the Coulomb interaction between the six poles and minimizing numerically the energy en the domain $(0, 2\pi)^3$.

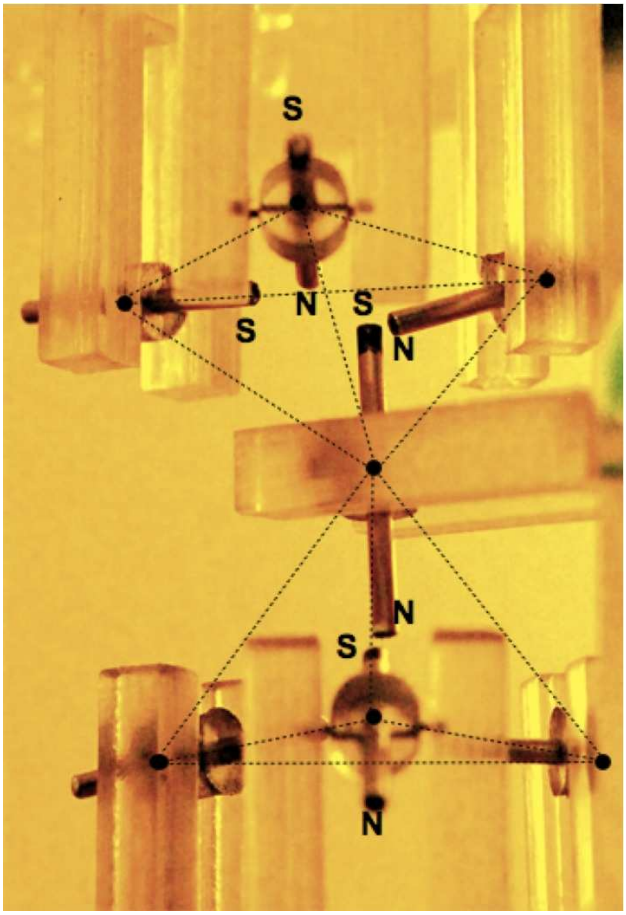

FIG. S12: A minimal 3-D generalization of our system. A tetrahedral configuration like the one found in the Pyrochlore lattice was created placing three acrylic plates one on the top of the other, the bottom and top plates contain three rotors defining an equilateral triangle and the middle plate contains one rotor located equidistant from the others.